ACS Sustainable Chemistry & Engineering

Research Article

Cite This: ACS Sustainable Chem. Eng. 2018, 6, 5162−5172

pubs.acs.org/journal/ascecg

Synergistic Performance of Composite Supercapacitors between Carbon Nanohorn and Conducting Polymer

Chia Chi Chang[†] and Toyoko Imae*[,†,‡]

[†]Department of Chemical Engineering and [‡]Graduate Institute of Applied Science and Technology, National Taiwan University of Science and Technology, Keelung Road, Taipei 10607, Taiwan

Supporting Information

ABSTRACT: This paper described the electrochmical behavior of composites of carbon nanohorns (CNHs) with conducting polymers [polyaniline (PA) and polypyrrole (PP)]. The materials at different weight ratios (monomer:CNH = 1:0, 1:0.33, 1:1, 1:3, and 0:1) were prepared by the in situ polymerization method. In the case of PA-series electrodes, the specific capacitance was a maximum (762 F/g at scan rate of 5 mV/s). Meanwhile, in the PP-series electrodes, the specific capacitance gradually decreased from 769 F/g at 5 mV/s for 1:0 (pyrrole:CNH) upon increasing the content of CNHs. However, the charge transfer resistance behaved completely contrary to the dependence of specific capacitance on the composite ratio. These electrochemical results revealed the strong synergistic effect between PA and CNHs of the PA-series composites, being facilitated by fast charge transfer, small internal resistance, and preferable mechanical properties and resulting in the improved capacitance performances. Furthermore, since the composites of both polymers at 1:3 (monomer:CNH) ratio showed an excellent capacitance retention, even after 5000 cycles, both polymers strengthened their cycling stability after the hybridization with CNHs.

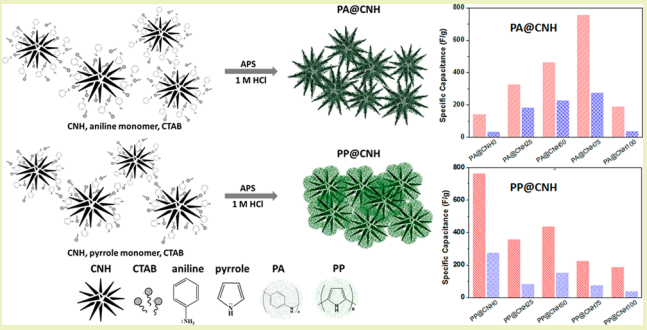

KEYWORDS: *Composite supercapacitor, Carbon nanohorn, Conducting polymer, Specific capacitance, Capacitance retention, Synergy effect*

INTRODUCTION

Nowadays, electrochemical capacitors are promising efficient electrical energy storage devices owing to their high power density, rapid charge−discharge, long cycle life, and high level of safety. They have found various applications in hybrid electric vehicles, portable devices, and memory backup systems that require electrical energy at high power levels in relatively short pulses.[1−3] Recent researchers have focused on the development of high-performance supercapacitor materials, such as carbon materials, conducting polymers, and metal oxides, and found that the composites of carbon material with conducting polymer have exhibited excellent electrochemical performance.[4−7] For instance, flowerlike polyaniline/graphene hybrids fabricated by an in situ chemical oxidative polymerization method have displayed a very high specific capacitance.[8] The hierarchical nanostructured polypyrrole/graphene composite has been also prepared via in situ chemical oxidative polymerization of pyrrole.[9] More importantly, it has been demonstrated that the composites can possess higher electrical conductivity, better structural mechanical stability, and greater enhancement on the capacitance properties than each component material.[10−13] It is noteworthy that the neutral aqueous electrolyte solution is becoming more popular, since it can eliminate the corrosion problem of acidic or basic electrolytes, it is environmentally friendly, inexpensive, and electrochemically stable, and, moreover, it can be easily handled in the laboratory without special conditions.[14−16]

Carbon nanohorns (CNHs) exhibit great promise as supercapacitor electrodes because of their distinguished electrical conductivity, wide surface area, and high ability of energy storage via two charge/storage mechanisms as well as novel physical properties.[17−19] Furthermore, among the conducting polymers, polyaniline (PA) and polypyrrole (PP) are also regarded as candidates for electrode materials of supercapacitors mainly due to their reversible control of conductivity by protonation and charge−discharge doping in addition to excellent capacity for energy storage, easy synthesis, good environmental stability, reproducibility, and relatively low cost.[20−22] Thus, combining the unique properties of CNH and conducting polymer will offer some attractive possibilities. This composite material would show novel effects, while each component maintains its intrinsic proprties. Although much research has been devoted to carbon material/conducting polymer composites, few studies have so far been performed for supercapacitors consisting of a composite of CNHs with PA:[23,24] The PA/CNH composites have been prepared by

Received: December 20, 2017
Revised: January 24, 2018
Published: February 15, 2018

DOI: 10.1021/acssuschemeng.7b04813
ACS Sustainable Chem. Eng. 2018, 6, 5162−5172

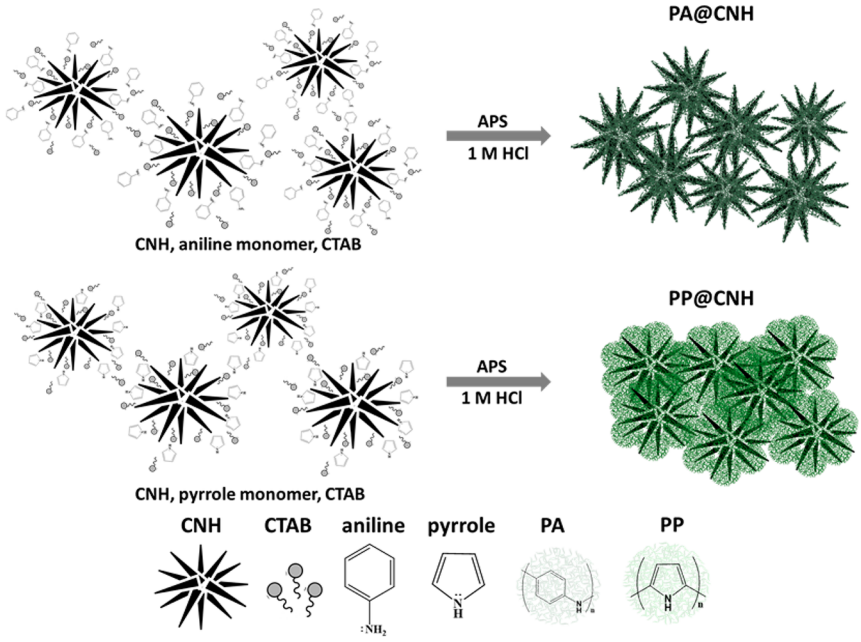

Figure 1. Illustration of the preparation process of the composites.

electrochemical nanofabrication[23] or in situ polymerization[24] and applied to the supercapacitance investigation.

The aim of this study is to report the electrochemical performances of conducting polymers affected by the amount of CNHs and the difference of contributions by conductive polymers with different structures on the electrochemical performances, since this type of the investigation has never been reported to the best of our knowledge. Herein, CNHs were complexated with polymers through a simple in situ polymerization of aniline and pyrrole. In addition to the characterization of the composites, including structural morphology, the electrochemical performances as electrodes of supercapacitors were investigated by cyclic voltammetry (CV), galvanostatic charge−discharge (GCD), and electrochemical impedance spectroscopy (EIS). The electrochemical results are expected to demonstrate the possible enhancement effects of capacitance and stability characteristics by the hybridization of CNH and conductive polymers, although such effects should depend on the kind of conductive polymers. Moreover, such an enhancement effect was discussed in conjunction with the composite structure. Thus, the present research will remarkably contribute to the advanced development of the supercapacitor.

EXPERIMENTAL SECTION

Materials and Characterization. CNH was purchased from NEC. Pyrrole (99%), aniline (99.5%), and ammonium persulfate (APS, 98+%) were obtained from Acros Organics, UK. Hexadecyltrimethylammonium bromide (CTAB) and a Nafion (perfluorinated resin) solution (5 wt % in lower aliphatic alcohols and 15−20% water) were purchased from Sigma-Aldrich. Indium−tin oxide (ITO) glass was purchased from AimCore Technology. Other reagents were of analytical grade, and all reagents were used as received. All the solutions were prepared using double-distilled deionized water.

The characterization was performed by transmission electron microscopy (TEM) (JEOL JSM-2000FX II) carried out at 120 kV, field emission scanning electron microscopy (FE-SEM) (JEOL JSM-6500F) at an accelerating voltage of 15 kV, and Fourier transform infrared (FTIR) absorption spectrometry (Nicolet thermo scientific 6700). Raman scattering spectra were measured on a Raman spectrometer (Horiba Jobin Yvon iHR550) with laser excitation of He−Ne 633 nm and power 10 mW. X-ray diffraction (XRD) patterns were characterized by a D2 PHASER X-ray diffractometer, and the analysis software was BRUKER, EVA V4.1. The thermal stability behavior was investigated using thermogravimetric analysis (TGA) (TA Q500 appliance) in the range of 25−1000 °C with a heating rate of 10 °C/min under nitrogen flow. Nitrogen physical adsorption was performed with a BELSORP-max instrument using N_2 as adsorbate at −196 °C. Before the adsorption measurements, the powders were degassed at 130 °C for 2 h. The specific surface area was calculated using the BET (Brunauer−Emmett−Teller) method from the N_2 adsorption isotherms within the relative pressure ranging from 0.05 to 0.25. The pore size distribution was obtained from the desorption isotherms using the Barrette−Joyner−Halenda (BJH) method.

Preparation of PA-Series and PP-Series Composites. Composite synthesis of CNHs and conducting polymers is as follows: The mixture of CNHs and CTAB (124 mg) in an aqueous 1 M HCl solution was sonicated for 1 h. Then aniline monomer (60 μL) was added and the mixture was stirred for 1 h at 0−5 °C. After the oxidizing agent APS (204 mg) in 1 M HCl (6.25 mL) was added dropwise, the mixture was kept stirring overnight at 0−5 °C. The resultant precipitate was filtered, washed several times with water and ethanol, and then dried overnight at 50 °C. The weight ratio of aniline to CNH was varied at 1:0.33, 1:1, and 1:3, and the resulting composites were named as PA@CNH25, PA@CNH50, and PA@CNH75, respectively. Similarly, composites of CNHs with PP were synthesized from pyrrole monomer by the same procedure, and resulting composites were named as PP@CNH25, PP@CNH50, and PP@CNH75. The same procedure was also followed to prepare polyaniline (PA) and polypyrrole (PP) without CNHs. The synthesis process of composites is illustrated in Figure 1.

Electrode Preparation and Electrochemical Measurement. For the preparation of working electrode, ITO glass (1 × 2 cm^2 piece) was cleaned by detergent followed by acetone, ethanol, and water and then treated by ultraviolet light (172 nm) under vacuum to remove a variety of organic contaminants from the ITO surface. The suspension of sample in ethanol (15 mg/mL) was sonicated for 2 h, and stirring continued for an additional 2 h after Nafion (250 μL) was added. For the preparation of the homogeneous thin film on ITO glass, the slurry of the mixture (150 μL) was spin-coated at 800 rpm for 10 s (step 1) and 1300 rpm for 30 s (step 2) on the cleaned ITO glass, dried at 50 °C, and supplied as a working electrode. The mass loading of the electrode materials was 0.06−0.08 mg/cm^2 on each working electrode.

DOI: 10.1021/acssuschemeng.7b04813
ACS Sustainable Chem. Eng. 2018, 6, 5162−5172

Electrochemical measurements were carried out in a 1 M NaCl electrolyte solution on a Zahner Zennium E electrochemical workstation using a typical three-electrode system, which was equipped with the working electrode prepared above, an Ag/AgCl reference electrode, and a Pt wire counter electrode. CV and GCD were measured at different scan rates ranging from 5 to 100 mV/s and at different current densities ranging from 1 to 10 A/g, respectively, within a potential window between −0.4 and 0.8 V. The EIS measurement was performed in the frequency range from 100 mHz to 100 kHz at an open circuit potential of 5 mV amplitude.

RESULTS AND DISCUSSION

Characterization of Composites. Conducting polymers were synthesized in an aqueous acid solution in the presence of CNHs, and TEM images of as-prepared composites (PA@CNH or PP@CNH) were compared with those of CNHs, PA (PA@CNH0), and PP (PP@CNH0), as shown in Figure 2. PA@CNH0 showed an irregularly shaped structure (see Figure 2a), but PP@CNH0 was nanowires of about 30 nm in diameter (see Figure 2e). However, the intrinsic structure of polymers was spoiled upon hybridizing with CNHs and became close to the spherical shape of CNH with a diameter at 80−100 nm (see Figure 2i), as observed in Figure 2b−d, and f−h. These results indicate that in situ polymerization occurrs on CNHs, and thus, polymers cover the CNH surface in the composites.

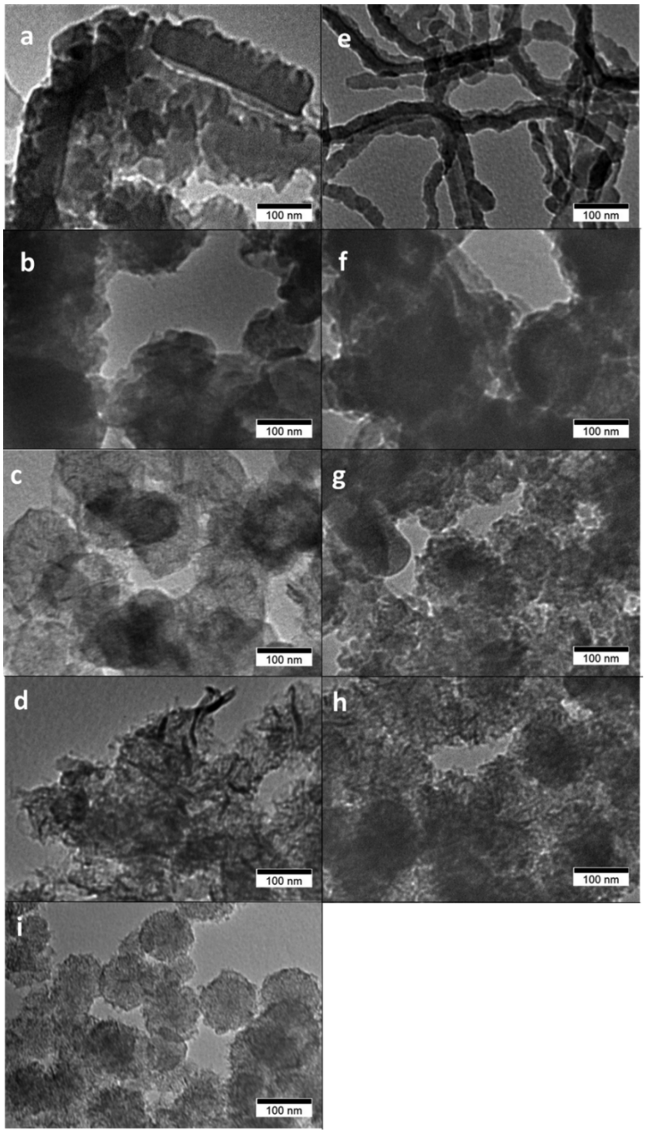

Figure 2. TEM images of (a−d) PA-series and (e−h) PP-series composites and (i) CNHs: (a and e) @CNH0, (b and f) @CNH25, (c and g) @CNH50, and (d and h) CNH75.

To further investigate the morphology of the composites, the characterization by FE-SEM was implemented. Figure 3 presents the FE-SEM images of intrinsic polymers and composites with CNHs (PA@CNH75 and PP@CNH75). In contrast to the morphologies of the polymers that were the amorphous texture of PA@CNH0 (Figure 3a) and the flexible wire structure of PP@CNH0 (Figure 3b), the morphologies of composites (Figure 3c,d) were fundamentally spherical, similar to CNHs (Figure 3e) and unlike the morphologies of pristine polymers, as observed in TEM images. The sizes (126−150 nm) of composite spheres seem slightly larger than that of pristine CNHs (80−100 nm), and this increase could be the deposition of polymers on CNHs, although such coating by polymers could not be identified from the TEM images.

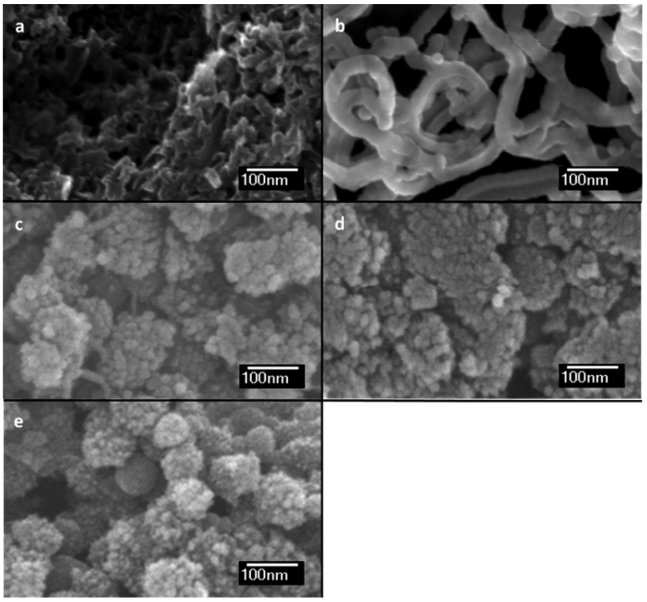

Figure 3. FE-SEM images of (a) PA@CNH0, (b) PP@CNH0, (c) PA@CNH75, (d) PP@CNH75, and (e) CNHs.

The chemical structures of CNHs, conducting polymers, and their composites were investigated by FTIR absorption spectroscopy. As shown in Figure 4 and listed in Table 1, the main characteristic bands of PA@CNH0 at 1568 and 1467 cm^{-1} are due to the C═C stretching vibration modes of the quinoid ring and benzenoid ring, respectively. The bands at 1290 and 1094 cm^{-1} can be attributed to the C−N stretching vibration and N═Q═N (Q represents the quinoid ring) modes, respectively.[25−27] For PP@CNH0, the main characteristic bands were at 1543 and 1454 cm^{-1}, which can be assigned to the C═C and C−N stretching vibration modes of pyrrole, respectively. The band at 1309 cm^{-1} is attributed to the C−N in-plane deformation vibration mode, and the bands at 1170 and 1031 cm^{-1} reflect the C−H stretching and C−H in-plane deformation vibration modes, respectively, of pyrrole rings.[28,29] The FTIR absorption bands of PA@CNH0 and PP@CNH0 were commonly observed, even in PA-series and PP-series composites, respectively. These results suggest the coexistance of polymer and CNH in the composites, although the

DOI: 10.1021/acssuschemeng.7b04813
ACS Sustainable Chem. Eng. 2018, 6, 5162−5172

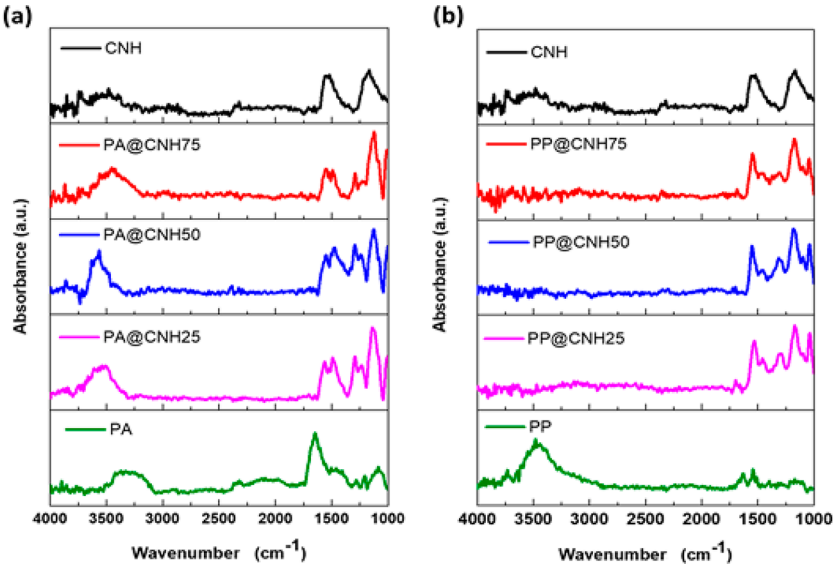

Figure 4. FTIR absorption spectra of (a) PA-series and (b) PP-series materials.

Table 1. FTIR Absorption Bands Observed for PA-Series and PP-Series Materials

assignment[a]	PA@CNH0	PA@CNH25	PA@CNH50	PA@CNH75	PA@CNH100
$\nu_{C=C}$ (quinoid ring)	1568	1476	1559	1571	1561/1167
$\nu_{C=C}$ (benzenoid ring)	1467	1500		1476	
ν_{C-N}	1290	1299	1287	1287	
N=Q=N (Q: quinoid ring)	1094	1121	1121	1121	
assignment[a]	PP@CNH0	PP@CNH25	PP@CNH50	PP@CNH75	PP@CNH100
$\nu_{C=C}$ (pyrrole)	1543	1547	1547	1547	1561/1167
ν_{C-N} (pyrrole and benzenoid ring)	1454	1453	1453	1453	
δ_{C-N}	1309	1311	1299	1299	
ν_{C-H} (pyrrole ring)	1170	1181	1169	1169	
δ_{C-H} (pyrrole ring)	1031	1039	1039	1039	

[a]Vibration modes: ν, stretching; δ, in-plane deformaion.

characteristic C=C stretching vibration band (1561 cm^{-1}) of CNH (polymer@CNH100) was not distinguished because this band was overlapped on the C=C stretching vibration band of polymers. Then the preferable complexation of polymers on CNH could occur by a strong attractive force like the $\pi-\pi$ stacking interaction of polymer precursor (monomer) with CNHs. Thus, CNHs could provide reaction sites for the nucleation polymerization of monomers on CNHs.[30,31]

Raman spectroscopy also can be used to investigate the chemical structure of CNH and its composites with conducting polymers (Figure 5). The main characteristic Raman bands of CNHs were observed at 1316 and 1584 cm^{-1}, which are attributed to D band (sp^2 bond vibration) and G band (sp^3 bond vibration), respectively. Meanwhile, Raman bands of conductive polymers were at 1369 and 1568 cm^{-1} for PA@CNH0 and 1383 and 1559 cm^{-1} for PP@CNH0, and these bands are characterized by their breadth, being different from the sharp bands of CNH. Even for polymer@CNH25, Raman bands of composites were mainly contributed by D and G bands of CNH, as judged from band positions and shape, indicating the strong contribution of Raman bands of CNHs in composites. Such contributions may be caused by the interaction between CNHs and the conducting polymer, such as $\pi-\pi$ stacking. Additionally, the intensity ratio of D and G bands (I_D/I_G) is generally related to the extent of disorder.[32−34] In both PA-series and PP-series composites, the I_D/I_G ratio was a maximum for polymer@CNH75. This result may be attributed to the increased sp^2 domains formed during the in situ polymerization process. All evidence from Raman results indicates that the conducting polymers have been grown onto the graphitic surface of CNHs with each affecting the other.

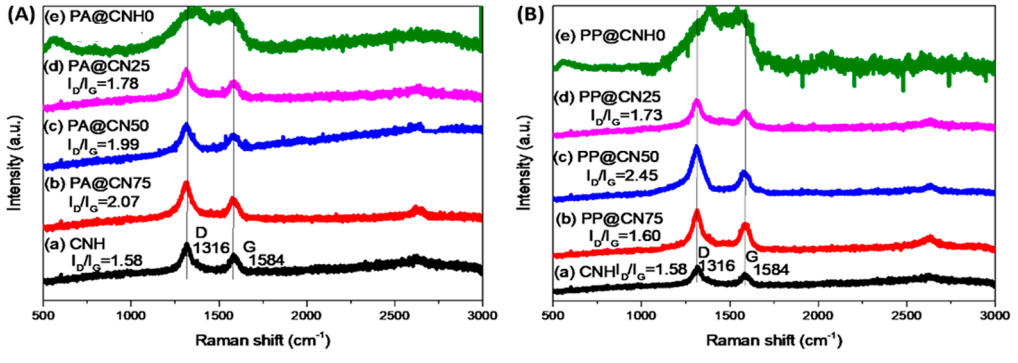

Figure 5. Raman scattering spectra of (a) PA-series and (b) PP-series composites.

DOI: 10.1021/acssuschemeng.7b04813
ACS Sustainable Chem. Eng. 2018, 6, 5162−5172

The XRD patterns of PA@CNH0, PP@CNH0, PA@CNH75, PP@CNH75, and CNH are shown in Figure 6. The

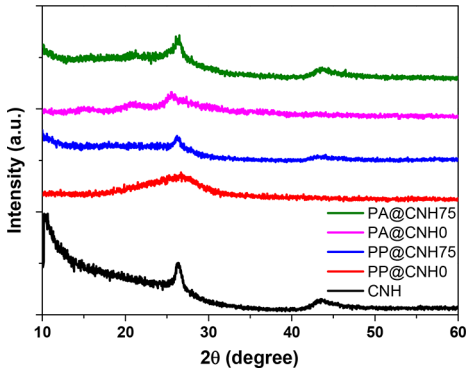

Figure 6. XRD patterns of PA@CNH0, PP@CNH0, PA@CNH75, PP@CNH75, and CNHs.

diffraction peaks of CNH were observed at 2θ = 26.34° and 43.51°, which can be assigned to the (002) and (100) crystal planes, respectively, of graphite-like structure. The XRD pattern of PA@CNH0 displayed three diffraction peaks at 2θ = 15.50°, 20.71°, and 25.57°, corresponding to (011), (020), and (200) crystal planes, respectively, of PA@CNH0 in its emeraldine salt form. In the XRD pattern of PP@CNH0, only one broad peak centered at 2θ = 26.51° was identified, and this peak is identical to that of amorphous PP@CNH0.[29,35,36] PA@CNH75 and PP@CNH75 composites exhibited diffraction peaks similar to those of CNHs, which makes up 75% in the composite. These results confirming the presence of CNHs in the composites.

TGA curves of PA-series and PP-series are shown in Figure 7. The CNHs possessed high thermal stability in the range from 25 to 1000 °C, and 86.25% of the mass was preserved, even at 1000 °C. In contrast, PA@CNH0 and PP@CNH0 showed multistep degradation until 920−940 °C and almost burned out

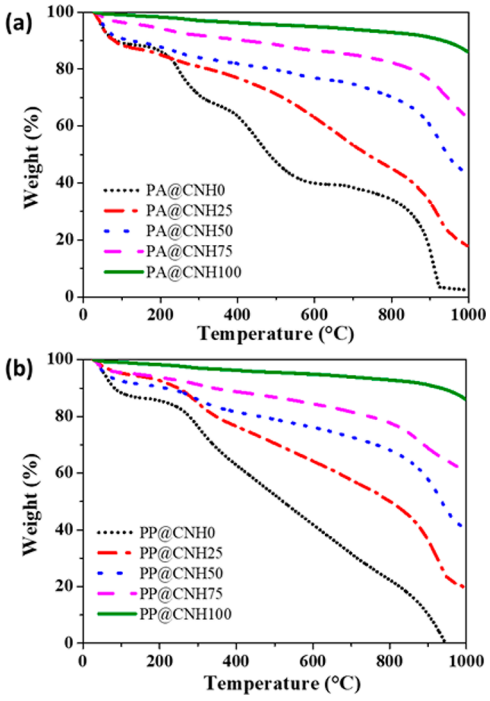

Figure 7. TGA curves of (a) PA-series and (b) PP-series materials.

above this temperature. TGA curves of composites suffered weight loss between amounts seen for pristine CNH and polymers, depending on their composition. Usually the composites show better thermal stability with less mass loss compared with the conductive polymers. Thus, the content of polymers in PA-series and PP-series composites can be evaluated from weight at 1000 °C. The obtained numerical values were 21, 50, and 73 wt % for PA@CNH25, PA@CNH50, and PA@CNH75, respectively, and 23, 47, and 70 wt % for corresponding PP-series composites. These observed values are reasonable in comparison with the calculated values.

Electrochemical Characterization of Composite Electrodes. The electrochemical behaviors of the PA-series and PP-series electrodes in 1 M NaCl were investigated by means of the CV and GCD. The CV curves of PA-series and PP-series electrodes, respectively, with different CNH contents are shown in Figure 8a,c and were measured at a scan rate of 50 mV/s. CV curves at different scan rates are shown in Figure S1 and Figure S2 of the Supporting Information (SI). The CV curves of these electrodes deviated from that of an idealized double-layer profile (rectangular shape) with an integrated CV area, indicating the improved capacitive behavior due to the Faradic reaction of the conductive polymers. Although the redox peaks were observed on the CV curve of pseudocapacitor electrodes constructed from intrinsic conductive polymers, such peaks were weak in the CV curves of composite electrodes because of the strong contribution of electric double-layer capacitance.

Values of specific capacitance C_s (F/g) were calculated according to the formula 1[37]

$$C_s = \int \frac{I}{m}\, dV/v\Delta V \tag{1}$$

where I (A) is the current, m (g) is the mass of active material, V (V) is the potential, ΔV (V) is the potential window, and v (V/s) is the scan rate. The specific capacitance of PA-series and PP-series electrodes is plotted in Figure 8, parts b and d, respectively, as a function of scan rate. The specific capacitance of all the electrodes decreased with an increase in scan rate due to the required time for ionic migration in porous portions of the electrode, although such a scan-rate-dependent decrease of specific capacitance was less for PP-series than PA-series, indicating better ionic migration in the former series.[21] The specific capacitance calculated was highest (762 F/g) for PA@CNH75 compared to other PA-series electrodes at the same scan rate (Figure 8b). By contrast, the highest specific capacitance among PP-series electrodes was 769 F/g for PP@CNH0, and the specific capacitance decreased with increasing CNH content in this series (Figure 8d).

To study further the capacitor performance, the GCD behaviors of the electrodes were examined at various current densities from 1.0 to 10 A/g (Figures S3 and S4, SI). Parts a and c of Figure 9 show the GCD of PA-series and PP-series electrodes, respectively, at the same current density (1.0 A/g). The GCD curves of all composites at whole current densities were almost shaped like a symmetric isosceles triangle, which is a typical capacitor behavior of supercapacitor.[38] The specific capacitance (C_s) was calculated using galvanostatic discharge curves according to eq 2[37]

$$C_s = Jt/\Delta V \tag{2}$$

where J (A/g) is the current density, t (s) is the discharge time, and ΔV (V) is the potential window. The specific capacitance

DOI: 10.1021/acssuschemeng.7b04813
ACS Sustainable Chem. Eng. 2018, 6, 5162−5172

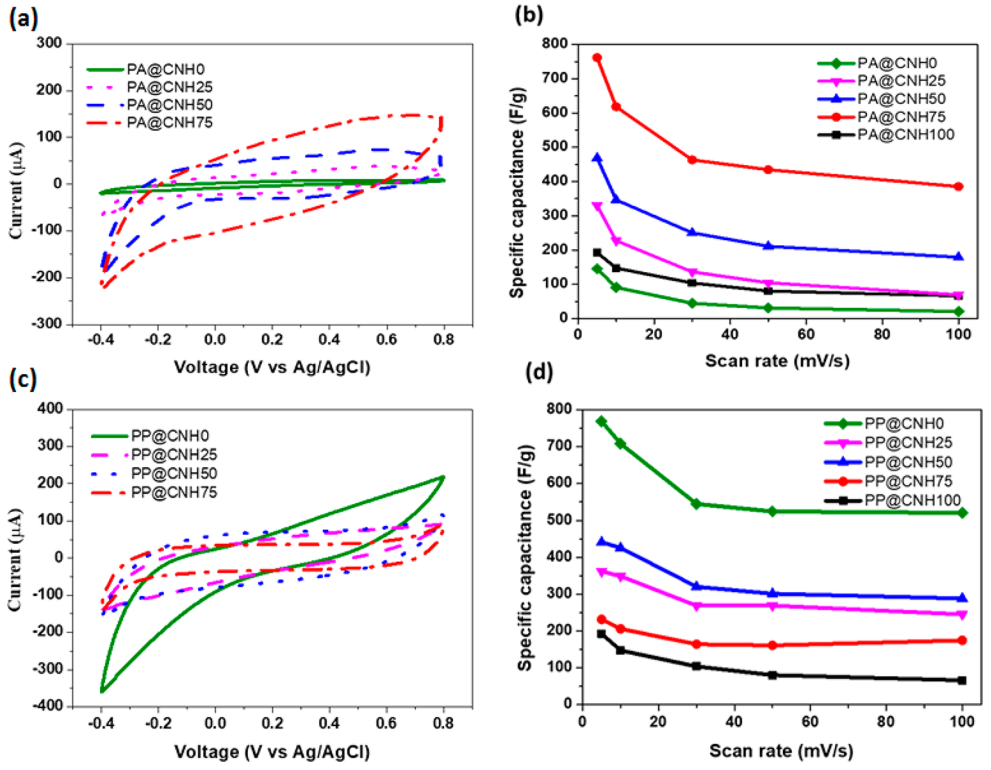

Figure 8. Electrochemical performances of (a and b) PA-series and (c and d) PP-series composites: (a and c) CV curves measured at a scan rate of 50 mV/s and (b and d) specific capacitance at different scan rates from 5 to 100 mV/s.

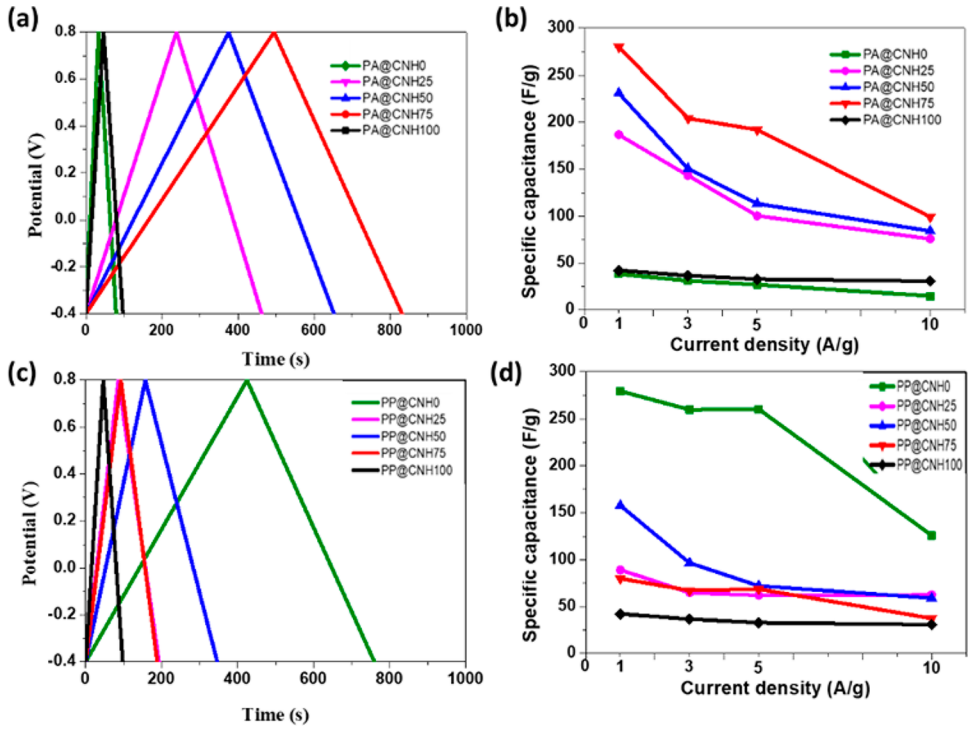

Figure 9. Electrochemical performances of (a and b) PA-series and (c and d) PP-series composites: (a and c) GCD curves measured at a current density of 1 A/g and (b and d) specific capacitance at different current densities from 1 to 10 A/g.

from GCD decreased with increasing current density (see Figure 9b,d) like the behavior of specific capacitance from CV. This is due to the delayed transport of electrolyte ions to the electrode surface, coming from porous portions of the electrode inaccessible at high current density.[38] At 1.0 A/g, the specific capacitance (280 F/g) of PA@CNH75 was much higher than values of other electrodes in the same series, and the progressive inclusion of CNHs from 25 to 75 wt % resulted in an increase in the characteristic charge−discharge time, which reflects an improvement of capacitance (Figure 9b).

DOI: 10.1021/acssuschemeng.7b04813
ACS Sustainable Chem. Eng. 2018, 6, 5162−5172

Meanwhile, a high specific capacitance of 280 F/g was observed for PP@CNH0, but the capacitance of the PP-series electrodes was lower than that of PP@CNH0 at the same current density (Figure 9d). The specific capacitance from GCD displayed similar behavior to that from CV for all electrodes, although the absolute values were different.

To investigate charge transport phenomena in porous materials and an equivalent electrical circuit in an electrode, EIS was measured at the open potential voltage in the frequency range between 100 mHz and 100 kHz at an amplitude of 5 mV (Figure 10). The equivalent circuit is

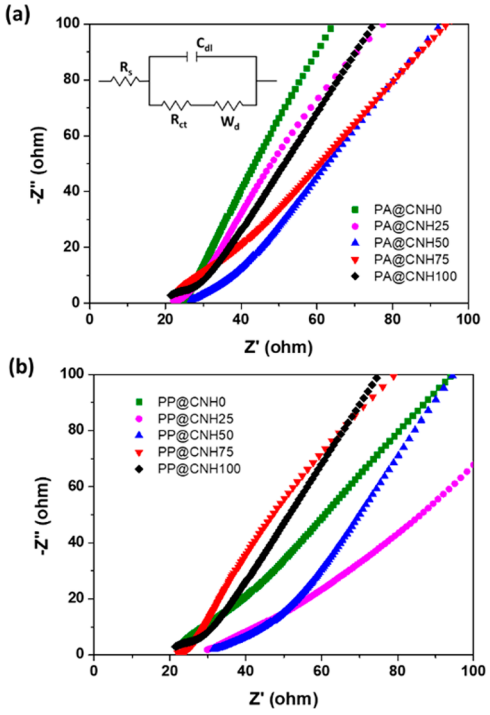

Figure 10. Nyquist plots of (a) PA-series electrodes and (b) PP-series electrodes at frequencies ranging from 100 mHz to 100 kHz. The inset in part a shows the equivalent electrical circuit.

composed of four elements of the solution resistance (R_s), the charge-transfer resistance (R_{ct}), the electrical double-layer capacitance (C_{dl}), and Warburg diffusion impedance (W_d), as displayed in the inset of Figure 10a. The evaluated values of charge-transfer resistance are listed in Table 2 with values of specific capacitance from CV at 5 mV/s and from GCD at 1 A/g.

The charge-transfer resistance of PA-series electrodes decreased down to the smallest value of PA@CNH75 with increasing CNH content, meaning that this composite has the quickest electron transport and fastest charge transfer at the electrode/electrolyte interface. On the other hand, the charge-transfer resistance of PP was very small, indicating the fast-enough charge transfer and better electrical conductivity of PP than other PP-series electrodes, since the charge-transfer resistance additively increased with increasing CNH content. The reason might be ascribed to its morphology of flexible entangled wires, which can provide ultrahigh passage for the charge transfer.[39]

The specific surface area and the pore size distribution of PA-series and PP-series composites were determined based on the BET and BJH models, respectively. All the isotherms possessed

Table 2. Comparison of Electrochemical Results from PA-Series and PP-Series Electrodes

electrode	S_{BET} ($m^2\ g^{-1}$)	V_{pore} ($cm^3\ g^{-1}$)	charge-transfer resistance (Ω)	specific capacitance (F/g) from CV at 5 mV/s	specific capacitance (F/g) from GCD at 1 A/g
PA@CNH0	39.7	0.284	6.213	145	38
PA@CNH25	31.8	0.303	2.995	330	187
PA@CNH50	56.6	0.485	2.143	469	231
PA@CNH75	85.7	0.378	1.333	762	280
PA@CNH100	419.6	1.343	5.788	193	42
PP@CNH0	121.5	0.914	1.036	769	280
PP@CNH25	47.1	0.388	2.749	362	89
PP@CNH50	196.6	0.909	2.367	441	158
PP@CNH75	133.5	0.521	3.238	231	80

the aspect of the type IV isotherm, being characteristic for porous materials (Figure 11). The numerical values of the surface area (S_{BET}) and the pore volume (V_{pore}) are listed in Table 2, as well as charge transfer resistance and specific capacitance. The S_{BET} and V_{pore} decreased after the growth of PA on the CNH surface, and this aspect was similar to that of the other carbon material/conducting polymer composites.[40−42] On the other hand, the dependence of the S_{BET} and V_{pore} of PP-series composites on the amount of CNH was not clear. The pore-size distribution curves derived from BJH analysis, as shown in Figure S5 (SI), indicated that the pore size averaged around 20 nm for polymer@CNH0 and polymer@CNH25, but the distinguishable pore-size distribution was not observed for polymer@CNH50 and polymer@CNH75.

Figure 12 plots all numerical values in Table 2 as a function of the weight ratio of polymer and CNH. The specific capacitance for PA-series electrodes increased with an increase of CNH content and maximized at PA@CNH75, but that for PP-series electrodes decreased with increasing CNH content. These CNH content dependencies are consistent with that of charge-transfer resistance. Thus, it can be noticed that the highly effective specific capacitance can promoted by the quick electron transport and the fast charge transfer at the electrode/electrolyte interface. However, the relationship of the specific capacitance to the surface area and the pore size/volume cannot be necessarily defined, because these parameters were gradually or slightly increased with an increase of the CNH content.

In addition, the cycle stability of PA@CNH75 and PP@CNH75 electrodes was assessed at a current density of 50 A/g, as shown in Figure 13. During increasing cycles, the capacitance slightly decreased for PA@CNH75 and PP@CNH75 electrodes, and this could be attributed to the degradation of the conductive polymer chains caused by the swelling/shrinkage of polymer chains during doping and dedoping processes of electrolytes and to the generation of small soluble oligomers, resulting in a mass loss for the polymers.[41,43] However, after 2000 cycles, the specific capacitance of PA@CNH75 retained 95% (of its initial specific capacitance) until 5000 cycles, and this value was more stable and higher than that of PP@CNH75, which retained 90% at 5000 cycles, due to the strong interaction between PA and CNH. It should be noted that the retentions of polymer@CNH75 are higher than intrinsic PA (92% at 4000 cycles) or PP (85% at 4000 cycles),[44] indicating the inhibition of degradation of polymers by

DOI: 10.1021/acssuschemeng.7b04813
ACS Sustainable Chem. Eng. 2018, 6, 5162−5172

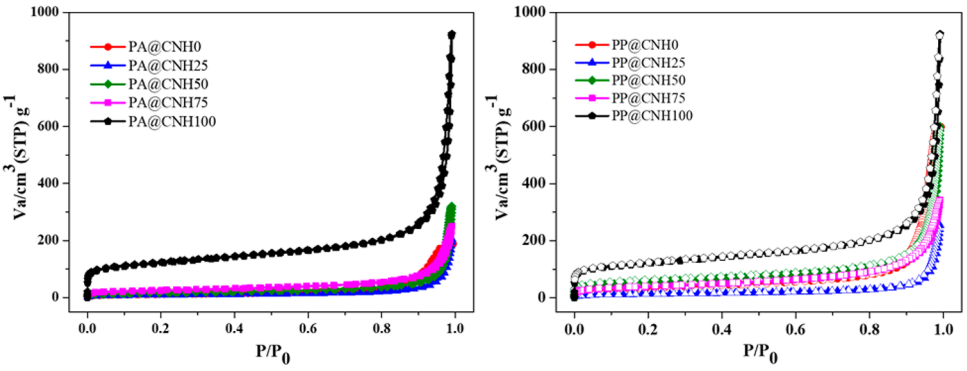

Figure 11. N_2 adsorption−desorption isotherms for PA-series and PP-series composites.

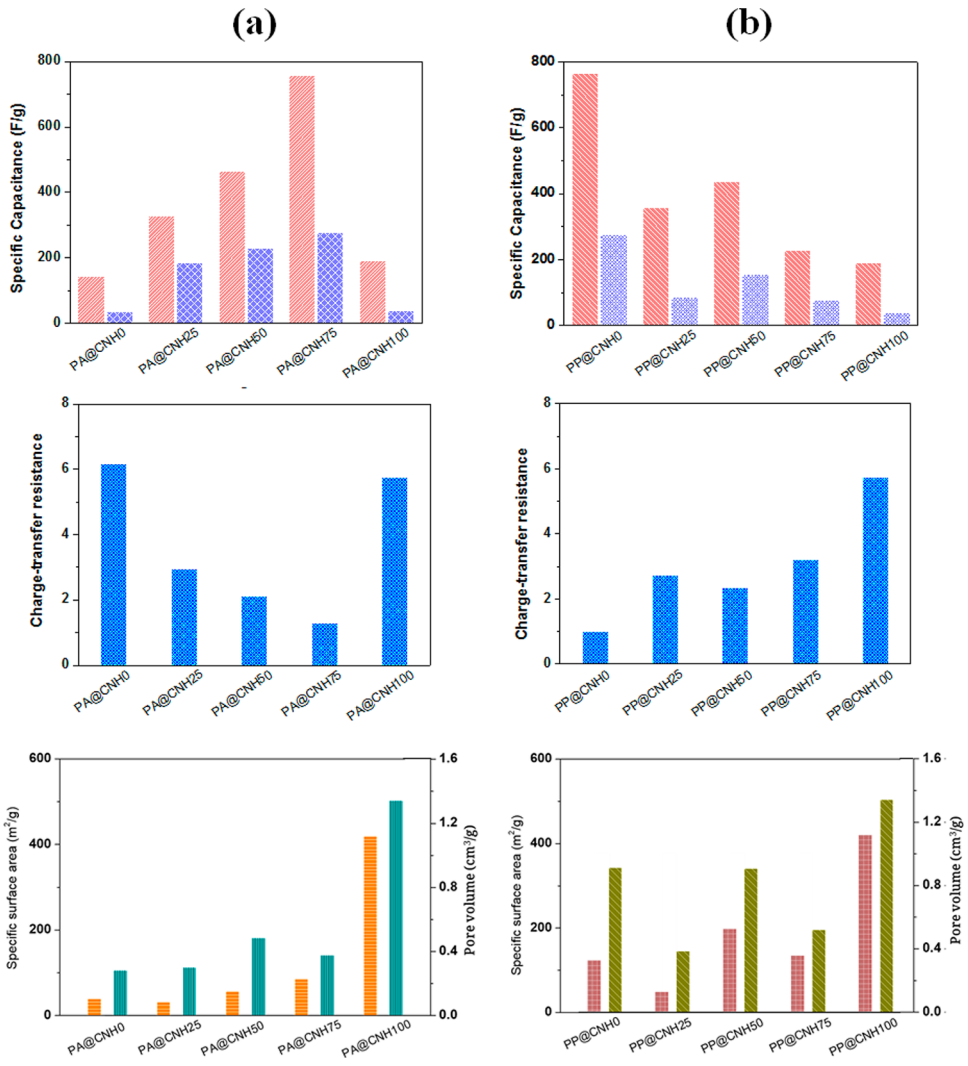

Figure 12. CNH content dependence of specific capacitance, charge-transfer resistance, and specific surface area/pore volume of (a) PA-series and (b) PP-series electrodes: pink, specific capacitance from CV; purple, specific capacitance from GCD; blue, charge-transfer resistance; orange/brown, specific surface area; green/dark brown, pore volume.

complexation with CNH involving the efficient enhancement of the mechanical strength of the composites after the complexation with CNH.

Furthermore, the morphology of the electrodes was compared for PA@CNH75 and PP@CNH75 before and after 5000 cycles, as shown in Figure 14. Before cycle stability, both electrodes have rough surfaces and composite nanoparticles were homogeneously distributed (Figure 14a,b). It should be noted that the morphologies of both electrodes strongly resemble those after 5000 cycles: There were no apparent changes in the well-kept nanostructured conducting polymer@CNH75 composites, in which the conducting polymers should be still covering the CNH surface.

DOI: 10.1021/acssuschemeng.7b04813
ACS Sustainable Chem. Eng. 2018, 6, 5162−5172

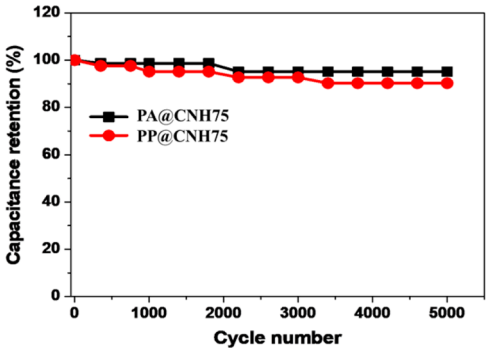

Figure 13. Cycling performance of PA@CNH75 and PP@CNH75 electrodes at a current density of 50 A/g.

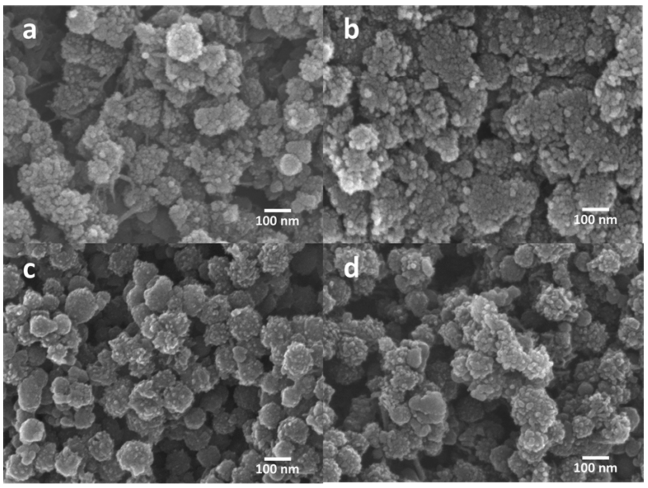

Figure 14. FE-SEM images of the electrodes (a and b) before the charge−discharge test and (c and d) after 5000 cycles: (a and c) PA@CNH75 and (b and d) PP@CNH75.

Thus, the above results of electrochemical characterizations demonstrate the synergistically enhanced supercapacitor properties of PA@CNH75 electrode, although PP was most excellent among PP-series electrodes with regard to specific capacitance. The reason for these different behaviors between the two polymers may be likely the contributions of a few characteristics, including the chemical structures of the polymers and the incorporation of polymers on the CNHs.

Both conducting polymers, PA and PP, have similar geometry, but their backbone chains provide different conductive and resonance effects and, consequently, different electron-donating properties.[45] In addition, although the aromatic ring planes of PP are slightly tilted with respect to the aromatic ring of CNH, PA fits to adsorb on the graphitic surface of CNH, because the phenylene rings of PA tend to easily colayer with CNH.[43,46−48] In other words, the $\pi-\pi$ stacking interaction between PP and CNH is significantly weaker than the interaction of CC double bonds of PA with π-electrons of the six-membered rings of CNH.[49,50] Moreover, the doping degree on PA (0.4−0.5) is usually higher than on PP (0.25−0.35).[51] That is, PA may facilitate the charge transfer process between the components of the system, increase the effective degree of electron delocalization due to its complete aromatic structure, and thus enhance the conductivity of the PA-series electrodes.[52,53] Therefore, we attribute the different behaviors between PA-series and PP-series composites to the resonance effect (the π-conjugated ring orientation effect) or the dopant ratio effect.

The interaction in the composites may facilitate the charge transfer process between the components of the system and increase the effective electron delocalization, thus ensuring easy charge/ion transport. Furthermore, the composite with CNH reduces the charge transfer resistance and increases the rate of electrochemical reaction in the bulk of the conducting polymer. As a result, the charge storage process in the supercapacitor is improved by rendering a high specific capacitance at a low scan rate and a low current density. Moreover, the existence of CNHs also can provide a robust support for the conducting polymer to enhance the cycling stability during charge−discharge.

In contrast to the many reports related to hybrid supercapacitors consisting of carbon materials with conducting polymers,[10,35,36] there are only a few reports for PA@CNH.[23,24] Wei et al.[23] have fabricated PA/CNH composite by electrochemical nanofabrication, and its specific capacitance was 168 F/g at 50 mV/s. This value is rather smaller than the products of the present work. Maiti and Khatua[24] have synthesized fiberlike PA/CNH composites using an in situ polymerization method and obtained the specific capacitance of 834 F/g at 5 mV/s, which is as high as the data in the present work. However, the cyclic stability of their composites was very low (84% at 500 cycles) in comparison to that of the present composites (99% at 500 cycles), indicting an unsatisfied improvement of the defect, that is, the low stability of the pseudocapacitor of conducting polymers in their composites, which is different from the present work.

CONCLUSIONS

In summary, PA-series and PP-series composites with different CNH contents were synthesized using in situ polymerization, and the composites have been proved to be effective charge collectors and electrode materials. Moreover, the present study demonstrated the synergistic performance depending on polymer species in composites of CNHs and conducting polymers: The PA-series composites proved the excellent positive synergistic effect between CNHs and PA. This is because the interaction in the composites is strongly based on the π-conjugated ring orientation effect. However, owing to the deviation of the aromatic ring orientation in PP from the six-membered rings of CNHs, the synergistic effect did not occur in the PP-series composites, although both composites exhibited capacitance retention superior to that of pristine polymers.

The different behaviors of composites with regard to the specific capacitance can be explained by the characteristics of the conducting polymers and their composites with CNHs. In the composites, PA can interact with CNHs by the strong $\pi-\pi$ stacking attraction force, which helps to reduce the contact resistance, enhances the electron transport at the electrode interface, and thus improves the electrical conductivity of the composites. In addition, PA can well and homogeneously adsorb on CNHs in the composite, which facilitates easy ion transfer through the composites but reduces the ionic diffusion route. Therefore, a strongly interconnected conducting network might be developed by the CNH and PA, and this development encourages more active electrochemical performances and is responsible for the high capacitance of the PA-series electrodes. For the PP-series electrodes, the highest capacitance performance of PP can be attributed to the relatively highly intertwined

DOI: 10.1021/acssuschemeng.7b04813
ACS Sustainable Chem. Eng. 2018, 6, 5162−5172

network of PP, which offers electrolyte ions a convenient pathway to the inside pores of electrode materials. However, the addition of CNH leads to a lowering of the device performance, because the ion pathway is blocked up. Consequently, the faster response to electrolyte ions and the superior rate performance of PA-series electrodes than PP-series electrodes may arise from the strongly interconnected conducting network and play a significant role in providing low-resistance pathways.

The present study offered us new insights into the interaction between conducting polymer and CNHs, moreover, providing us the effective selection of novel electrode materials for supercapacitors with excellent activity.

■ ASSOCIATED CONTENT

Supporting Information

The Supporting Information is available free of charge on the ACS Publications website at DOI: 10.1021/acssuschemeng.7b04813.

CV and GCD curves with various scan rates and current density, respectively, and pore dize distributions for PA-series and PP-series materials (PDF)

■ AUTHOR INFORMATION

Corresponding Author

*E-mail: imae@mail.ntust.edu.tw. Tel: +886-2-2730-3627.

ORCID

Toyoko Imae: 0000-0003-2731-1960

Notes

The authors declare no competing financial interest.

■ ACKNOWLEDGMENTS

This research was partially supported by Ministry of Science and Technology (MOST 106-2221-E-011-121-), Taiwan. We thank Dr. M. M. M. Ahmed for the support on measurements of Raman, XRD and BET.

■ REFERENCES

(1) Sarangapani, S.; Tilak, B.; Chen, C. P. Materials for Electrochemical Capacitors Theoretical and Experimental Constraints. *J. Electrochem. Soc.* **1996**, *143*, 3791−3799.

(2) Baisden, A. C.; Emadi, A. Advisor-Based Model of a Battery and an Ultra-Capacitor Energy Source for Hybrid Electric Vehicles. *IEEE Trans. Veh. Technol.* **2004**, *53*, 199−205.

(3) Simon, P.; Gogotsi, Y. Materials for Electrochemical Capacitors. *Nat. Mater.* **2008**, *7*, 845−854.

(4) Zhang, L. L.; Zhao, X. S. Carbon-Based Materials as Supercapacitor Electrodes. *Chem. Soc. Rev.* **2009**, *38*, 2520−2531.

(5) Liu, C.; Li, F.; Ma, L. P.; Cheng, H. M. Advanced Materials for Energy Storage. *Adv. Mater.* **2010**, *22*, E28.

(6) Yu, G.; Xie, X.; Pan, L.; Bao, Z.; Cui, Y. Hybrid Nanostructured Materials for High-Performance Electrochemical Capacitors. *Nano Energy* **2013**, *2*, 213−234.

(7) Liu, X.; Shang, P.; Zhang, Y.; Wang, X.; Fan, Z.; Wang, B.; Zheng, Y. Three-Dimensional and Stable Polyaniline-Grafted Graphene Hybrid Materials for Supercapacitor Electrodes. *J. Mater. Chem. A* **2014**, *2*, 15273−15278.

(8) Ke, F.; Liu, Y.; Xu, H.; Ma, Y.; Guang, S.; Zhang, F.; Lin, N.; Ye, M.; Lin, Y.; Liu, X. Flower-Like Polyaniline/Graphene Hybrids for High-Performance Supercapacitor. *Compos. Sci. Technol.* **2017**, *142*, 286−293.

(9) Fan, X.; Yang, Z.; He, N. Hierarchical Nanostructured Polypyrrole/Graphene Composites as Supercapacitor Electrode. *RSC Adv.* **2015**, *5*, 15096−15102.

(10) Béguin, F.; Frackowiak, E. *Carbons for Electrochemical Energy Storage and Conversion Systems*; CRC Press, 2009.

(11) Qu, G.; Cheng, J.; Li, X.; Yuan, D.; Chen, P.; Chen, X.; Wang, B.; Peng, H. A Fiber Supercapacitor with High Energy Density Based on Hollow Graphene/Conducting Polymer Fiber Electrode. *Adv. Mater.* **2016**, *28*, 3646−3652.

(12) Zhou, H.; Han, G. One-Step Fabrication of Heterogeneous Conducting Polymers-Coated Graphene Oxide/Carbon Nanotubes Composite Films for High-Performance Supercapacitors. *Electrochim. Acta* **2016**, *192*, 448−455.

(13) Gabe, A.; Mostazo-López, M. J.; Salinas-Torres, D.; Morallón, E.; Cazorla-Amorós, D. 8. Synthesis of Conducting Polymer/Carbon Material Composites and Their Application in Electrical Energy Storage. In *Hybrid Polymer Composite Materials*; Woodhead Publishing: 2017; pp 173−209.

(14) Chen, P.-C.; Shen, G.; Shi, Y.; Chen, H.; Zhou, C. Preparation and Characterization of Flexible Asymmetric Supercapacitors Based on Transition-Metal-Oxide Nanowire/Single-Walled Carbon Nanotube Hybrid Thin-Film Electrodes. *ACS Nano* **2010**, *4*, 4403−4411.

(15) Zhong, C.; Deng, Y.; Hu, W.; Qiao, J.; Zhang, L.; Zhang, J. A Review of Electrolyte Materials and Compositions for Electrochemical Supercapacitors. *Chem. Soc. Rev.* **2015**, *44*, 7484−7539.

(16) Ahmed, M. M.; Imae, T. Electrochemical Properties of a Thermally Expanded Magnetic Graphene Composite with a Conductive Polymer. *Phys. Chem. Chem. Phys.* **2016**, *18*, 10400−10410.

(17) Zhang, Z.; Han, S.; Wang, C.; Li, J.; Xu, G. Single-Walled Carbon Nanohorns for Energy Applications. *Nanomaterials* **2015**, *5*, 1732−1755.

(18) Karousis, N.; Suarez-Martinez, I.; Ewels, C. P.; Tagmatarchis, N. Structure, Properties, Functionalization, and Applications of Carbon Nanohorns. *Chem. Rev.* **2016**, *116*, 4850−4883.

(19) Yáñez-Sedeño, P.; Campuzano, S.; Pingarrón, J. *Carbon Nanostructures for Tagging in Electrochemical Biosensing: A Review. C* **2017**, *3*, 3.

(20) Sen, T.; Mishra, S.; Shimpi, N. G. Synthesis and Sensing Applications of Polyaniline Nanocomposites: A Review. *RSC Adv.* **2016**, *6*, 42196−42222.

(21) González, A.; Goikolea, E.; Barrena, J. A.; Mysyk, R. Review on Supercapacitors: Technologies and Materials. *Renewable Sustainable Energy Rev.* **2016**, *58*, 1189−1206.

(22) Basnayaka, P. A.; Ram, M. K., A Review of Supercapacitor Energy Storage Using Nanohybrid Conducting Polymers and Carbon Electrode Materials. In *Conducting Polymer Hybrids*; Kumar, V., Kalia, S., Swart, H. C., Eds.; Springer International Publishing, 2017; pp 165−192.

(23) Wei, D.; Wang, H.; Hiralal, P.; Andrew, P.; Ryhänen, T.; Hayashi, Y.; Amaratunga, G. A. Template-Free Electrochemical Nanofabrication of Polyaniline Nanobrush and Hybrid Polyaniline with Carbon Nanohorns for Supercapacitors. *Nanotechnology* **2010**, *21*, 435702.

(24) Maiti, S.; Khatua, B. Polyaniline Integrated Carbon Nanohorn: A Superior Electrode Materials for Advanced Energy Storage. *eXPRESS Polym. Lett.* **2014**, *8*, 895.

(25) Blinova, N. V.; Stejskal, J.; Trchová, M.; Prokeš, J.; Omastová, M. Polyaniline and Polypyrrole: A Comparative Study of the Preparation. *Eur. Polym. J.* **2007**, *43*, 2331−2341.

(26) Zhou, D.; Li, Y.; Wang, J.; Xu, P.; Han, X. Synthesis of Polyaniline Nanofibers with High Electrical Conductivity from Ctab−Sdbs Mixed Surfactants. *Mater. Lett.* **2011**, *65*, 3601−3604.

(27) Babu, V. J.; Vempati, S.; Ramakrishna, S. Conducting Polyaniline-Electrical Charge Transportation. *Mater. Sci. Appl.* **2013**, *4*, 27057.

(28) Stejskal, J.; Omastová, M.; Fedorova, S.; Prokeš, J.; Trchová, M. Polyaniline and Polypyrrole Prepared in the Presence of Surfactants: A Comparative Conductivity Study. *Polymer* **2003**, *44*, 1353−1358.

(29) Mi, H.; Zhang, X.; Ye, X.; Yang, S. Preparation and Enhanced Capacitance of Core−Shell Polypyrrole/Polyaniline Composite Electrode for Supercapacitors. *J. Power Sources* **2008**, *176*, 403−409.

DOI: 10.1021/acssuschemeng.7b04813
ACS Sustainable Chem. Eng. 2018, 6, 5162−5172

(30) Mittal, V. *In-Situ Synthesis of Polymer Nanocomposites*; John Wiley & Sons, 2011.
(31) Li, X.; Zhong, Q.; Zhang, X.; Li, T.; Huang, J. In-Situ Polymerization of Polyaniline on the Surface of Graphene Oxide for High Electrochemical Capacitance. *Thin Solid Films* **2015**, *584*, 348−352.
(32) Butler, S. Z.; et al. Progress, Challenges, and Opportunities in Two-Dimensional Materials Beyond Graphene. *ACS Nano* **2013**, *7*, 2898−2926.
(33) Yuge, R.; Bandow, S.; Nakahara, K.; Yudasaka, M.; Toyama, K.; Yamaguchi, T.; Iijima, S.; Manako, T. Structure and Electronic States of Single-Wall Carbon Nanohorns Prepared under Nitrogen Atmosphere. *Carbon* **2014**, *75*, 322−326.
(34) Shao, D.; Hou, G.; Li, J.; Wen, T.; Ren, X.; Wang, X. Pani/Go as a Super Adsorbent for the Selective Adsorption of Uranium(Vi). *Chem. Eng. J.* **2014**, *255*, 604−612.
(35) Yan, J.; Wei, T.; Shao, B.; Fan, Z.; Qian, W.; Zhang, M.; Wei, F. Preparation of a Graphene Nanosheet/Polyaniline Composite with High Specific Capacitance. *Carbon* **2010**, *48*, 487−493.
(36) Gawri, I.; Khatta, S.; Singh, K. P.; Tripathi, S. K. Synthesis and Characterization of Polyaniline as Emeraldine Salt. *AIP Conf. Proc.* **2015**, *1728*, 020287.
(37) Yu, A.; Chabot, V.; Zhang, J. *Electrochemical Supercapacitors for Energy Storage and Delivery: Fundamentals and Applications*; CRC Press, 2013.
(38) Conway, B. E. *Electrochemical Supercapacitors: Scientific Fundamentals and Technological Applications*; Springer Science & Business Media, 2013.
(39) Oueiny, C.; Berlioz, S.; Perrin, F.-X. Carbon Nanotube−Polyaniline Composites. *Prog. Polym. Sci.* **2014**, *39*, 707−748.
(40) Lei, Z.; Chen, Z.; Zhao, X. S. Growth of Polyaniline on Hollow Carbon Spheres for Enhancing Electrocapacitance. *J. Phys. Chem. C* **2010**, *114*, 19867−19874.
(41) Zheng, L.; Wang, Y.; Wang, X.; Li, N.; An, H.; Chen, H.; Guo, J. The Preparation and Performance of Calcium Carbide-Derived Carbon/Polyaniline Composite Electrode Material for Supercapacitors. *J. Power Sources* **2010**, *195*, 1747−1752.
(42) Okan, B. S.; Zanjani, J. S. M.; Letofsky-Papst, I.; Cebeci, F. Ç.; Menceloglu, Y. Z. Morphology-Controllable Synthesis and Characterization of Carbon Nanotube/Polypyrrole Composites and Their Hydrogen Storage Capacities. *Mater. Chem. Phys.* **2015**, *167*, 171−180.
(43) Zhou, Y.; Qin, Z.-Y.; Li, L.; Zhang, Y.; Wei, Y.-L.; Wang, L.-F.; Zhu, M.-F. Polyaniline/Multi-Walled Carbon Nanotube Composites with Core−Shell Structures as Supercapacitor Electrode Materials. *Electrochim. Acta* **2010**, *55*, 3904−3908.
(44) Devadas, B.; Imae, T. Effect of Carbon Dots on Conducting Polymers for Energy Storage Applications. *ACS Sustainable Chem. Eng.* **2018**, *6*, 127.
(45) Reynolds, J. R. *Conjugated Polymers: Processing and Applications*; CRC Press, 2006.
(46) Choi, J.; Chipara, M.; Xu, B.; Yang, C.; Doudin, B.; Dowben, P. Comparison of the Π-Conjugated Ring Orientations in Polyaniline and Polypyrrole. *Chem. Phys. Lett.* **2001**, *343*, 193−200.
(47) Zhou, Y.-k.; He, B.-l.; Zhou, W.-j.; Huang, J.; Li, X.-h.; Wu, B.; Li, H.-l. Electrochemical Capacitance of Well-Coated Single-Walled Carbon Nanotube with Polyaniline Composites. *Electrochim. Acta* **2004**, *49*, 257−262.
(48) Shaktawat, V.; Jain, N.; Saxena, R.; Saxena, N.; Sharma, K.; Sharma, T. Temperature Dependence of Electrical Conduction in Pure and Doped Polypyrrole. *Polym. Bull.* **2006**, *57*, 535−543.
(49) Street, G.; Clarke, T.; Geiss, R.; Lee, V.; Nazzal, A.; Pfluger, P.; Scott, J. Characterization of Polypyrrole. *J. Phys. Colloq.* **1983**, *44*, C3-599−C3−606.
(50) Zheng, Q.; Xue, Q.; Yan, K.; Hao, L.; Li, Q.; Gao, X. Investigation of Molecular Interactions between Swnt and Polyethylene/Polypropylene/Polystyrene/Polyaniline Molecules. *J. Phys. Chem. C* **2007**, *111*, 4628−4635.
(51) Li, Y. *Organic Optoelectronic Materials*; Springer, 2015; Vol. *91*.
(52) Hunter, C. A.; Lawson, K. R.; Perkins, J.; Urch, C. J. Aromatic Interactions. *J. Chem. Soc., Perkin Trans. 2* **2001**, 651−669.
(53) Wang, R.-X.; Huang, L.-F.; Tian, X.-Y. Understanding the Protonation of Polyaniline and Polyaniline−Graphene Interaction. *J. Phys. Chem. C* **2012**, *116*, 13120−13126.

DOI: 10.1021/acssuschemeng.7b04813
ACS Sustainable Chem. Eng. 2018, 6, 5162−5172